ISSN: 0067-2904

Optimizing Application of UAV-Based SfM Photogrammetric 3D Mapping in Urban Areas

Abbas Mohammed Noori [1], Ali Salah J. Al-Saedi [2], Fanar M. Abed [3*]

[1] *Department of Surveying Technologies Engineering, Technical Engineering College of Kirkuk, Northern Technical University, Kirkuk 36001, Iraq*

[2] *Surveying Department, Technical Institute of Amara, Southern Technical University, Misan 62001, Iraq*

[3] *Surveying Engineering Department, College of Engineering, University of Baghdad, Baghdad 10001, Iraq*

Received: 2/3/2023 Accepted: 15/5/2023 Published: 30/5/2024

Abstract

In recent years, the extensive need for high-quality acquisition platforms for various 3D mapping applications has rapidly increased, especially in sensor performance, portability, and low cost. Image-based UAV sensors have overwhelming merits over alternative solutions for their high timeline and resilience data acquisition systems and the high-resolution spatial data they can provide through extensive Computer Vision (CV) data processing approaches. However, applying this technique, including the appropriate selection of flight mission and image acquisition parameters, ground settings and targeting, and Structure from Motion- Multi-View Stereo (SfM-MVS) post-processing, must be optimized to the type of study site and feature characteristics. This research focuses on optimizing the application of UAV-SfM photogrammetry in an urban area on the east bank of the Tigris River in the north region of Iraq following optimized data capturing plan and SfM-MVS photogrammetric workflow. The research presented the practical application of optimized flight planning, data acquisition, image processing, accuracy analysis, and evaluation based on ground truth targets designed for the proposed optimal routine. This includes investigating the influence of the number and distribution of GCPs, flying heights, and processing parameters on the quality of the produced 3D data. The research showed the potential of low-budget and affordable UAV devices to deliver robust 3D products in a relatively short period by demonstrating the value of UAV-based image techniques when contributed to CV algorithms. The results showed powerful outcomes with validation errors reaching a centimeter-level from 100 m flying height when applying the optimized flight plan settings and the appropriate selection of the number and distribution of GCPs. The study established a streamlined UAV mapping procedure, demonstrated the viability of UAV use for 3D mapping applications, offered suggestions for enhancing future applications, and offered clues as to whether or not UAVs could serve as a viable alternative to conventional ground-based surveying techniques in accurate applications.

Keywords: Remote sensing, Low-cost UAV, Structure from Motion, Multi-View Stereo, Photogrammetry, Flight Planning, DEM, Quality Analysis.

أمثلية تطبيق نمذجة الخرائط ثلاثية الابعاد باعتماد المسح التصويري وفقا لنظريات الـ *SfM* باستخدام الطائرة المسيرة في المناطق الحضرية

عباس محمد نوري[1]، علي صلاح السعيدي[2]، فنار منصور عبد[3]*

*Email: fanar.mansour@coeng.uobaghdad.edu.iq

[1]قسم المساحة، الكلية التقنية الهندسية، الجامعة التقنية الشمالية، كركوك، العراق
[2]قسم المساحة، المعهد التقني، الجامعة التقنية الجنوبية، ميسان، العراق
[3]قسم هندسة المساحة، كلية الهندسة، جامعة بغداد، بغداد، العراق

الخلاصة

في السنوات الأخيرة ، ازدادت الحاجة الشديدة لمنصات جمع البيانات عالية الجودة لمختلف تطبيقات انتاج الخرائط ثلاثية الأبعاد بسرعة فائقة ، لا سيما من حيث أداء المستشعر وسهولة الاستخدام والتكلفة المنخفضة. تتمتع انظمة الطائرات المسيرة التي تحمل انظمة تصوير مرئية بمزايا هائلة مقارنة بالحلول البديلة للجدول الزمني في الانتاج وأنظمة الحصول على البيانات المرنة والبيانات المكانية عالية الدقة التي يمكن أن توفرها من خلال مناهج معالجة البيانات اوتوماتيكيا بالاعتماد على نظريات رؤية الحاسبة. ومع ذلك ، فإن تطبيق هذه التقنية بما في ذلك الاختيار المناسب لنوع المستشعر ومواصفاته ، وعوامل الحصول على الصور وإعداداتها ، يالاضافة الى الإعدادات الأرضية الواجب اتباعها ونوع الاهداف وطبيعتها ضمن منطقة الدراسة ، والمعالجة بالاعتماد على نظريات Structure from Motion– Multi View Stereo (SfM–MVS) ، بالاضافة الى التحقق من صحة المخرجات يحتاج إلى نظريات الامثلية وفقًا لنوع موقع الدراسة وخصائص العوارض فيه. يركز هذا البحث على تحسين تطبيق المسح التصويري للطائرات المسيرة اعتمادا على نظريات الـSfM في منطقة حضرية تقع على الضفة الشرقية لنهر دجلة في المنطقة الشمالية من العراق عبر اعتماد خطة الطيران الامثل لجمع البيانات ومعالجتها اوتوماتيكيا باستخدام نظريات SfM–MVS. قدم البحث التطبيق العملي للتخطيط الأمثل للطيران ، والحصول على البيانات ، ومعالجة الصور ، وتحليل الدقة والتقييم على أساس أهداف حقيقية والمصممة للروتين الأمثل المقترح. يتضمن ذلك تحليل النتائج في تأثير عدد نقاط التحكم في الشبكة وتوزيعها ، وارتفاع الطيران ، جنبًا إلى جنب مع عناصرالمعالجة المعتمدة على جودة البيانات ثلاثية الأبعاد المنتجة. يُظهر البحث إمكانات استخدام نظريات رؤية الحاسبة عبر استخدام الطائرة المسيرة منخفض التكلفة وبأسعار معقولة والتحكم اوتوماتيكيا لتقديم منتجات ثلاثية الأبعاد ذات جودة عالية في فترة زمنية قصيرة نسبيًا من خلال إظهار قيمة تقنيات الصور المستندة إلى الطائرات المسيرة عند المساهمة بنظريات الـ SfM–MVS. يظهر اعتماد الامثلية في حساب عناصر الطيران واعداد الخطة اوتوماتيكيا نتائج مشجعة مع أخطاء التحقق التي تصل إلى مستوى السنتيمترات من ارتفاع طيران 100 متر عند تطبيق الاختيار الأمثل لعدد وتوزيع GCPs. أنشأت الدراسة إجراءً مبسطًا لانتاج خرائط من الطائرات المسيرة ، وأظهرت جدوى استخدامها لتطبيقات انتاج الخرائط ثلاثية الأبعاد ، وقدمت اقتراحات لتعزيز التطبيقات المستقبلية ، وقدمت أدلة حول ما إذا كانت الطائرات المسيرة يمكن أن تكون بديلاً قابلاً للتطبيق لتقنيات المسح الأرضية التقليدية في تطبيقات دقيقة.

1. Introduction

Computer vision (CV) has allowed photogrammetry to develop into a robust and frequently used technology for diverse 3D applications [1]. Structure from motion (SfM) is a CV image-based technique that shows a powerful solution over traditional photogrammetry in 3D mapping due to its reliability, realistic, and powerful application solution. However, the capacity to rebuild a scene with no prior knowledge of camera positions and orientation in 3D space and the deployment of fixed reference marks in the scene is the key to this approach's simplicity, power, and portability [2]. As an alternative, a series of overlapping images and an iterative solution of bundle adjustment (non-linear solution) can be used to determine the camera locations in post-processing. However, to set the scale and elevation of the generated 3D data, a Multi-View-Stereo (MVS) mathematical approach is needed alongside several GCPs to rebuild the realistic 3D scene from the optimized camera settings delivered from the previous SfM workflow [3]. In the SfM method, algorithms locate similar images and generate "key spots" that serve as processing checkpoints. As new solutions are added to the set's bundle adjustment database, those matches are fine-tuned repeatedly via least-square minimization [4]. However, the MVS technique automatically generates 3D tie points from

the retrieved key points. Although the reconstructed scene has neither size nor geographic limitations at this stage, if a set of 3D ground control points with known coordinates are visible and assigned, a 3D similarity transformation can align the dataset to a real-world coordinate system [5].

In order to be easily spotted in the field, GCPs should have a distinct shape and color from their surroundings [6]. It is possible to use natural landmarks, but man-made objects with great comparison and a well-defined centroid are more convenient to deploy in practice [7]. Surveying the center location of these man-made objects using conventional geodetic methods is then required so that it may be used to optimize camera locations and orientations. One of the various methods used by SfM is the Scale Invariant Feature Transform (SIFT) for recognizing objects [8], [9]. Important landmarks in the photos are identified automatically; these landmarks are represented by feature descriptors that are most robust to variations in translation, rotation, and scaling and partially robust to lighting variations [10]. The actual complexity, difference, and brightness of the scene to be captured and the image's sharpness and resolution determine the number of key points per image to be extracted [10].

Consequently, it impacts the precision of the reconstructed model [11]. There is no universal rule for how many shots should be taken or how much overlap should apply between images because every scenario is unique. However, it is recommended to use at least three images per crucial point and take as many photos as possible [10], [12]. The processing time, however, will grow proportionally with the amount of captured photos and photographs. The ground sampling distance (GSD) is also a factor in accuracy that should be calculated carefully to set the flight plan parameters [13], [14], [15]. To follow up, this research aims to present an optimized workflow of topographic mapping in urban sites. The optimization includes flight planning, camera settings, ground targeting, data capturing, and post-processing stages toward optimal outcomes. The research also provides a verification analysis regarding accuracy standards in low-cost projects.

2. Literature Review

To bring the methodical study into the investigation, previous works must be reviewed to create facts and extend new assumptions. Most compiled literature focuses predominantly on the UAV's hardware rather than investigating the optimized workflow and analyzing parameters. Hence, only limited studies are available to investigate UAV products upon flight plan optimization in urban sites. In this context, [16] has used UAVs to investigate producing high-quality 3D products to record an archaeological site. They revealed that UAVs could stand in front of digital tools to document the past over analog techniques like measuring tapes and tachymeters in Cultural Heritage (CH) and archaeology [17]. However, they claimed that the image processing stages must be automated so that the many outputs, often sketches, maps, ortho-images, and 3D models, can be made available without delay. Later, [18] investigated the latest developments in image-based automatic processing methods for photogrammetric applications. They captured 100 images over an archaeological site in Veio, Italy, of a block have a middling scale of 1:4400 with a mean flying altitude of 35 m of l cm GSD. They found these outcomes resulted in about 330,000 picture correspondences, which were then decreased to around 18,000 to facilitate a more rapid computation of the bundle correction. The horizontal and the vertical validation error was calculated based on five selected marks in the scene which were approximately 3.5, and 7 cm in horizontal and vertical directions respectively. They revealed that these variations are very undoubtedly attributable to the fact that the target coordinates in the photos were measured traditionally.

Nonetheless, the results were accurate enough for archaeological purposes. The Successive Mic-Mac technique used to measure the surface area over 40 million generated point clouds.

On the other hand, [19] studied the accuracy of DEM generated based on the potential processing of digital images captured by Canon imagery sensor equipped in the MAVinci Sirius I-UAV platform. In the [19] study, the investigation was based on the conditions where data would typically be collected during a field study. They utilized a total of 1042 ground control points for use in the photogrammetric processing and as high-precision reference data to extract the DEMs. They discovered that various parameters of the interpolated DEMs can be highly affected by the accuracy of the imagery sensor angle and its deviation. In conclusion, the superiority of the sensor orientation was shown to increase whenever more GCPs were assigned during the aero-triangulation process.

Further, [20] examined the quality of DSM generated from UAV photogrammetry following SfM-MVS workflow to monitor coastal shorelines. They used a fully automatic work frame to map and monitor the development of beaches and dunes. The complete CV processing workflow was implemented using Agisoft Photoscan CV software, including automatic aerial triangulation, camera calibration, and the subsequent development of the DS models to emphasize the best positional precision for the entire dataset. It was possible to obtain high-resolution DSMs and georeferenced imagery with high temporal resolution using a low-cost UAV platform.

Furthermore, [21] built a system that has been rigorously tested for accurate modeling in various environments, including harsh conditions of an open-pit gravel mine. In different mapping contexts, the accuracy of the outputs is evaluated using varying numbers of ground control points, distributions, and types. They also investigate the mapping implementation process using direct and indirect geo-referencing approaches. Experiments showed an absolute horizontal accuracy of 1.55m and vertical accuracy of 3.16m with a geo-referencing approach. However, results were improved to reach 0.4cm and 1.7cm in horizontal and vertical accuracy, respectively, through indirect geo-referencing. When comparing their method to manual target identification, the authors found about 81% improvement in calibration accuracy following their proposed method based on in-house hardware systems and software programs. They claimed that by utilizing this method, the association between Interior Orientation Parameters (IO) and Exterior Orientation Parameters (EO) of the images in an inappropriate imaging network could be reduced by 60%.

Consequently, [22] claimed numerous issues compromised the reliability of UAV photogrammetry's outputs. The number, distribution, shape, and accurate measure of the ground targets may influence the quality level of the extracted realistic 3D clouds. Therefore, edge and stratified distributions were employed for testing until a critical mass of GCPs was reached. They suggested that increasing the number of GCPs can lead to more precise results but not necessarily be accurate. As a result, they improved the vertical accuracy to reach 0.062m when the optimum combination for optimizing horizontal accuracy was chosen. The horizontal accuracy reached 0.045m if the best possible settings were chosen to maximize the vertical precision. Then, various projects focused on assessing the absolute accuracy level through the root-mean-square-error (RMSE) analysis and the Multiscale Model to Model Cloud Comparison (M3C2) [23]. In [23], they investigate the number and the distribution of GCPs and their effects on accuracy and cost in corridor mapping projects. They assess the two variables through RMSE and M3C2 statistical analysis. They achieved 0.031 and 0.081m horizontal and vertical accuracy, respectively, with fewer GCPs. They claimed that placing GCPs on both sides of a linear feature, such as a road in an identical or zigzag pattern, can

optimize the results of fieldwork costs. The best results were achieved by stagger-placing GCPs on either roadside with an offset distance between them or by placing a matching pair of GCPs at both corridor ends. Later, [24] examines four different GCP configurations and their relationship with GSD value to deliver optimal geospatial data in a low-cost UAV mapping project. In this research, the horizontal and the vertical accuracy of the resulting UAV solution were investigated by comparing the locations of 21 GCPs with the reference ground truth measured by RTK DGPS method. Given these findings, and assuming compliance with industry-reference accuracy criteria standards (ASPRS), the outputs found to deliver 4-5 cm accuracy in horizontal and vertical scale respectively those reveals to be double to triple the GSD value.

As traditional methods are becoming challenging to deploy with the continuous development of new technologies and yielding a time-consuming process, using UAVs to conduct field surveys in multi-terrain area surveys is becoming more potential to adopt. However, difficulties might acquire in representing terrain and ground features. However, with the advent of low-cost UAVs, scholars are trying to take advantage of these feasible and potential platforms to use them as alternative tools for 3D mapping. To follow up, this research presents an optimized practical application of a low-cost UAV image-based platform for 3D mapping in urban sites, following the latest Artificial Intelligent (AI) techniques of SfM photogrammetry. The objective of this research is to assess the UAV-SfM photogrammetric products based on optimized configurations of the flight plan, data capture, ground targeting, data post-processing parameters, and the accuracy of the produced three-dimension model in order to deliver a foundation for future studies and base for corporations that aim to integrate UAVs with commercial. Furthermore, comparing the outcomes of the models created with those extracted using traditional techniques in terms of accuracy, cost, and time.

3. Study Area

The study site chosen to deploy this research was an urban region located on the eastern bank of the River Tigris, south of Kirkuk province in the north of Iraq (Latitude 35° 23' 54" north, Longitude 44° 20' 44" east). The selected region spans around 240m×120m and is part of the Kirkuk Technical Engineering campus founded in 1998, see Figure 1. The area was selected for various ground feature types, including the built-up areas of the same governmental building shapes with approximately 7m height, residential blocks, local roads, and some vegetation areas.

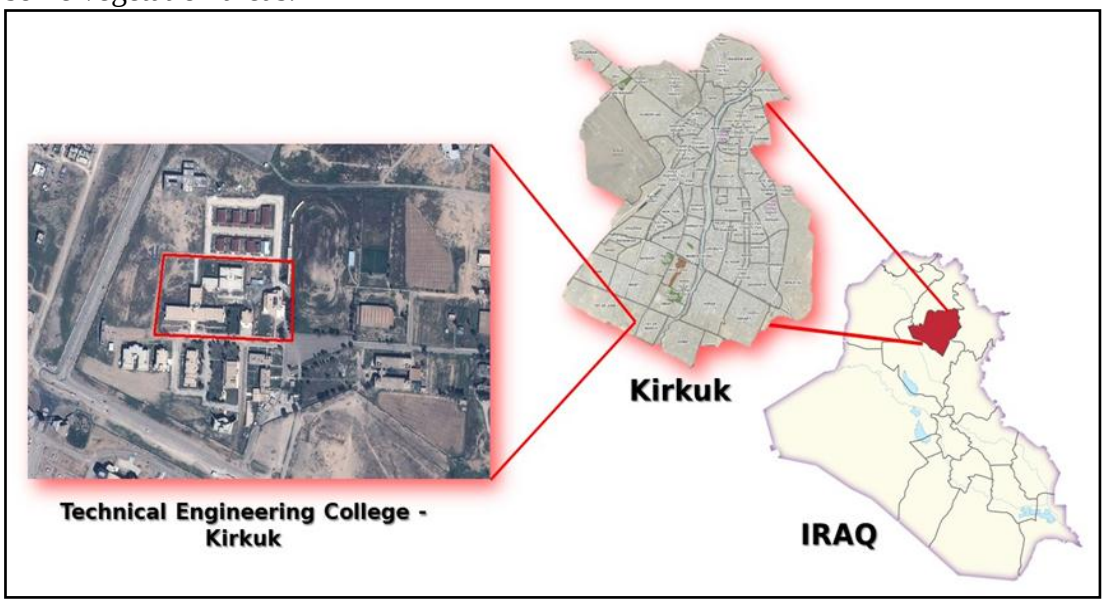

Figure 1: The study area's geographic location.

4. Methodology

The research was deployed on a local situation study area in Iraq. In other words, the study looks into a modern phenomenon in its actual setting. This study aims to discover what accuracy level can obtain based on optimized configurations from low-cost UAV sensors following SfM-MVS photogrammetry algorithms. The collected images were shifted to a CV environment and treated with a profitable photogrammetric software, the so-called Metashape from Agisoft, to create 3D photogrammetric products. The delivered accuracy was assessed by judgment to location quantities from a DGPS and Total station device measurements. This allowed us to validate the outputs from the configured routine according to ground truth reference data to show potential. See the technical configured workflow in Figure 2 for further details.

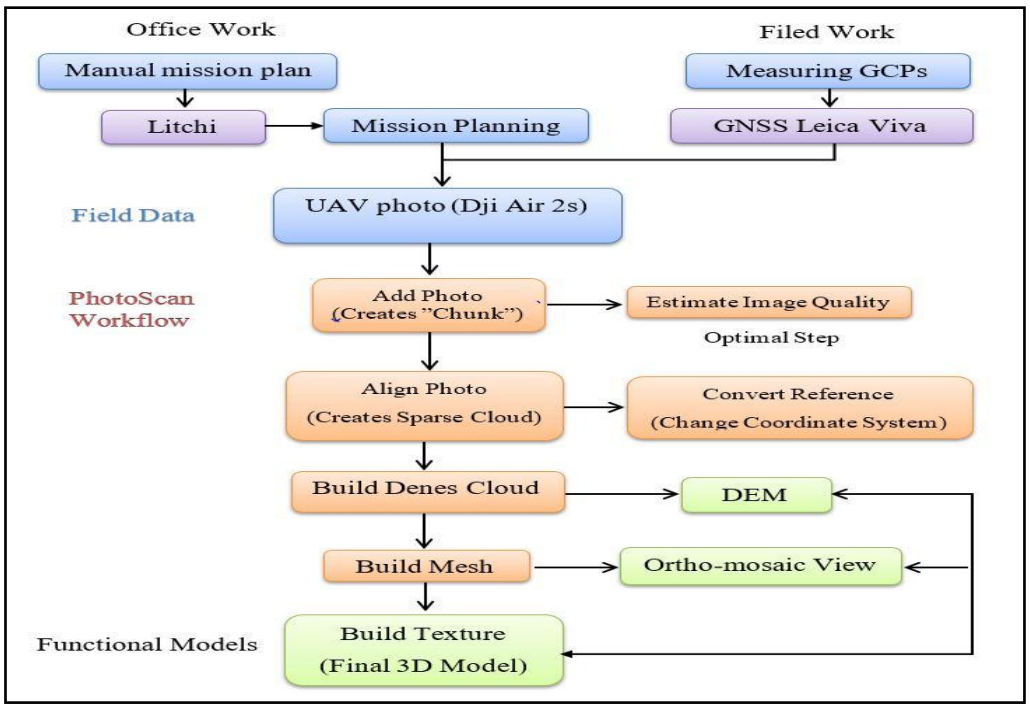

Figure 2: Technical methodological workflow operations.

4.1 Utilized Tools

A DJI AIR 2s is a low-cost UAV platform used in this research; Figure 3. Due to its small size and lightweight, the UAV was much more straightforward to utilize and manipulate than highly equipped high-cost aerial platforms. The image sensor of this UAV is 1″ CMOS of 20 MP and 2.4 μmpixel size. The camera lens has a 35mm focal length (22mm equivalent), f/2.8 aperture, and 0.6-∞ range (www.dji.com). Table 1. Shows the Dji Air 2s technical specifications. A Leica's Viva GNSS device was used for the GCP measurements, which offers various options for specific needs. With Viva GNSS, it may choose a solution to manage every task, from a fully integrated mission to a suite of individual components.

Figure 3: The DJI Air 2s UAV used in this research.

Table 1: DJI Air 2s technical specifications (www.dji.com).

Function	Parameter
Model	DJI Air 2s
Max Flight time	20-27 mins
Navigation	GPS + GLONASS
Battery	3500 mAh
Camera	20 MP, 1-inch CMOS sensor, 13.2×8 mm sensor size, 8.38 mm focal length, 5472×3078 pix image dimension
Weight	595 g
Flight applications	DJI fly + Litchi (Paid)
Max. Speed	68 km/h
Max. distance	12 km

4.2. Flight Planning

The precision of aerial photogrammetry projects depends on the number of factors that must be considered during planning. The errors obtained in the outputs within the horizontal plane reflect the planimetric accuracy achieved, whereas those obtained in the vertical plane refer to the accuracy achieved in the depth-extracted computations. Estimates are utilized for the flight height that could be employed, and the percentage of front and side overlap between images because these values may be computed before the mission starts based on optimization planning considerations toward optimal outcomes. A significant factor usually set to select the optimal altitude value for the mission is the spatial resolution or GSD, which is defined by the size of the image's pixel reflected in the earth's natural size [3].

4.3. Optimizing Mission Parameters

Altitude is one of the most influential factors when planning flight missions because it affects key vectors like depth accuracy and spatial resolution (GSD). The GSD value was calculated as demonstrated in Equation 1 [25].

$$GSD = \frac{(\text{flight altitude x sensor size})}{(\text{focal length x image height and/or width})} \quad (1)$$

The mission altitude affects post-processing timeframes and data storage by determining how many photos were projected to survey the scene. The UAV has a built-in camera with fixed sensor settings; the focal length, sensor size, image dimensions, and pixel size are defined as the image quality, which will be fixed in all proposed missions, regardless of the camera altitude. The number of flight lines and the camera trajectories pre-mission were calculated as illustrated in Equations (2-8), [3] [26]:

$$(W) = w \times S.N \quad (2)$$
$$(L) = l \times S.N \quad (3)$$
$$(SP) = (W) \times ((100 - PS)/100) \quad (4)$$
$$(NFL) = (Width/SP) + 1 \quad (5)$$
$$(B) = (L) \times ((100 - PE)/100) \quad (6)$$
$$(NIM) = (Length/B) + 1 \quad (7)$$
$$TNI = NFL \times NIM \quad (8)$$

Where:
W (eq:2) is the image ground coverage in width; L is the image ground coverage in length; w (eq:4) is the image width which may equal to image length in the case of a square image; S.N is the image scale number; SP is the distance between flight lines; PS is the amount of side lap; NFL is the number of flight lines; B is the distance between two consecutive images (Airbase); PE is the amount of end lap; NIM is the number of images per flight line; and TNI is the total number of images for the entire flight mission.

Following literature recommendations in urban areas [6], an 80% forward and side overlap percentage was adopted across photographs to maintain the optimal feature coverage. However, the other flight mission parameters were configured, as illustrated in Table 2.

The photo ground coverage was calculated to be (160×90m). At the same time, the side and front overlap was 80%. In addition, the air base, which reflects the distance between exposure Stations (B), was calculated to be equal to 18 m (90×(1-%80)). Furthermore, the distance between flight lines (W) was calculated to be equal to 32m (160×(1-%80)).

Table 2: GSD Calculator and flight mission configurations.

Symbol	Value	Details
Sh	13.2	Camera sensor height (mm)
Sw	8	Camera sensor width (mm)
FR	8.38	Camera focal length (mm)
H	100	Flying height (m)
imH	5472	Image height (pixels)
imW	3078	Image width (pixels)
GSD	2.88	Ground Sampling Distance (cm/pixel)
Dw	158	Image footprint width (m)
Dh	89	Image footprint height (m)

4.4. Flight Mission Application

The Litchi app for DJI UAVs (www.Litchi.com) was used to manage the Autopilot system in the UAV platform. Litchi is a popular UAV app, easy to use, as it has many impressive

features, giving the user more control to add to the flying experience. This autonomous UAV app has many customization features and advanced control options [27]. Litchi was the first App to allow UAV pilots to set and save missions on their desktops. Their waypoints mission engine is highly intuitive and can be controlled by beginners and professionals. Following previous optimization calculations, Table 3. shows the parameter settings used with the Litchi capture app in this research mission. This mission planner is compatible with all devices, including Mac/ PC, and the user can synchronize the mission across other devices in case of extreme fliers. Figure 4 illustrates a mobile view of flight missions over the selected case study.

Table 3: Flight mission parameters.

Parameter	Value
Front overlap	%80
Side overlap	%80
Altitude	100 m.
Flight speed	15 Km/h
Photo Capture Interval	5 sec.
Gimbal Pitch	-90 deg.

Figure 4: Flight mission in Litchi App (Mobile view).

4.5. Field Work

Typically, in photogrammetry, GCPs were desirable to set in the field to configure the scale and the elevation of the generated 3D model through geo-referencing. Different types of GCPs meet the needs of any photogrammetric data processing. The GCPs were created to stand out clearly against the background and have their center pinpointed to be ease targeted

in the post-processing office work phase. They were usually designed to be flat plates with some cross or point tag [28]. The size of the targets depends on the flight altitude and the camera used. Later in the processing stage, the targets were marked to rescale and optimize, aligning the images into the same coordinate system as the GCPs. Fifteen ground control points (GCPs) were installed and measured using a Leica Viva GS15 GNSS, using the universal UTM reference. By linking the photos to the actual site, GCPs improve the reliability of the extracted model. SfM-MVS processes become more reliable when more than three GCPs are utilized [29]. Theoretically, the outcomes could be affected by factors such as the number, size, and distribution of GCPs. It is also significant to remember that these GCPs must be very apparent on the images to be recognized and picked up readily during the automatic CV photogrammetry processing. As a result, it is essential to consider the ground resolution and flying height while designing the size of GCPs. Figure 5 shows the target size and type used, which was 60×60cm of wooded type. Whereas Figure 6 shows the GCP locations and distribution in the study site.

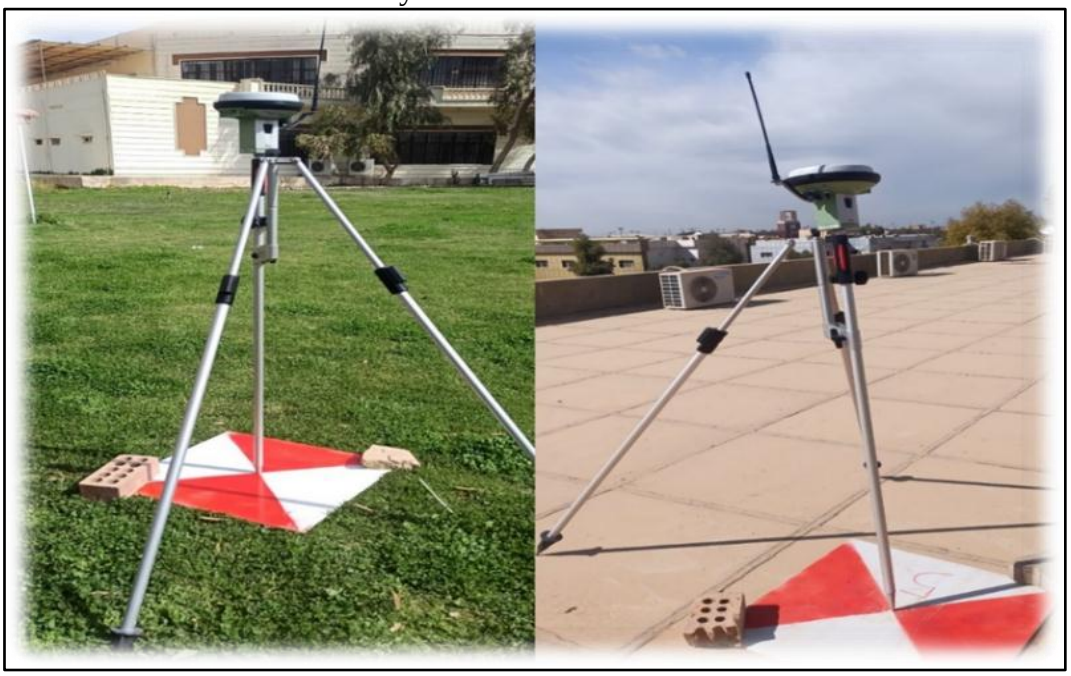

Figure 5: GCP targets in the study site.

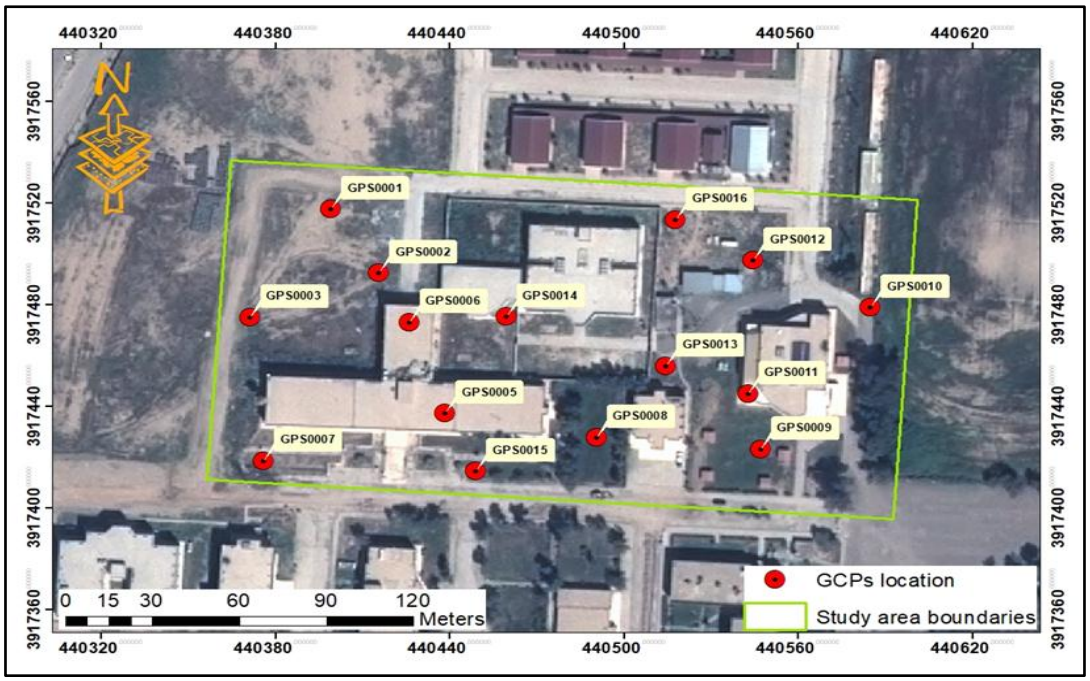

Figure 6: GCP Locations and distribution in the study site.

4.6. Flight Time and Data Acquisition

After the flight mission was created according to the specifications of the existing camera, the flight altitude and the image overlap percentage were set to the flight mission (Litche). The ground control points were installed, and their coordinates were measured and post-processed using OPUS online positioning GPS post-processing service (www.geodesy.noaa.gov.OPUS) based on Leica Viva GS15 GNSS previous measurements. The survey day was partially cloudy on March 17, 2022, at 10:00 AM, and the wind speed was between 5 km to 10 km, considered perfect conditions according to the size of the UAV used and its low-cost specifications. After connecting the UAV control device with the mobile device, the flight plan was downloaded through the Litchi app and started the automatic data capture process according to the designed plan using the nadir camera setting (the direction of the camera lens is perpendicular to the ground). Following this, more than 60 aerial photos were obtained in less than 10 min of flying. Table 4 illustrates the flight plan configuration specified in this mission plan.

Table 4: Configurations of the flight plan specified in the research flight mission.

Parameter	Value
Flight duration	6 min.
No. of flight lines	6
Total No. of photos	62 photos

4.7. Data Post-Processing

Agisoft Metashape is a multi-step processing work frame that processes data from aerial or terrestrial image platforms. The camera calibration was optimized based on the GPS navigator sensor available within the utilized UAV. This help to correctly define the approximate values of the pixel and sensor sizes based on defining the camera type and its related focal length. Later, aligning images was implemented to correctly register the images from different camera positions and orientations in one SfM approach. This was applied

under the workflow menu, which opens a dialog box to specify the parameters of the automatic aligning process. The resulting display in the Model window is a sparse point cloud that shows the generated key points to define the depth information of the 2D data and represent the general shape of the model (object or scene). Most UAVs use GPS/INS to assign location information to each image captured with the built-in camera. The ground control points were used to locate the camera positions in order to optimize the camera positions. The View Sources button will display the cameras' longitude, latitude, altitude, and other metadata within the reference pane. Selecting a toggle allows the user to change the coordinate system to a more common or area-appropriate system, such as WGS84, a common survey standard that was selected. Post-Processing includes the following stages: Dense Cloud, Mesh, Texture, DEM, and Ortho-mosaic.

5. Results and Discussions

The study findings highlight the advantages and disadvantages of employing SfM-MVS photogrammetry based on optimized UAV mission parameters as an alternative to more conventional means of surveying and re-creating objects at different scales. After processing the data, the results were analyzed and evaluated. Sixty images were processed and later geo-tagged using ground control points based on ground truth reference data. Table 5. shows the results constraints of UAV-based SfM-MVS photogrammetry in this research.

Table 5: Results constraints of using UAV-based SfM-MVS photogrammetric approach.

Number of Cameras	Number of Tie Points	Depth Map Parameters	Number of Dense Clouds	Number of Polygon Faces in 3D Model	DEM Resolution
62	39,638	High Quality, Mild Filtering	39,171,402	7,834,274	5.67 cm/pix

When comparing the observed data to the reference data for validation purposes, the normalized RMSE (NRMSE) was calculated [30]; see Equations 9 and 10. Variation between the derived values from the UAV photogrammetry result and the reference dataset at certain GCPs was used to measure the computed validation accuracy. Before the image-collecting phase, RTK GPS observations were used to collect reference values, which were adjusted following the least squares routine. The RMSE was then determined by validating these values to the ground truth adjusted measures.

$$\mathrm{RMSE_x} = \sqrt{\frac{\sum(\mathrm{X_{UAV}}-\mathrm{X_{GPS}})^2}{\mathrm{n}}}\ ;\ \mathrm{RMSE_y} = \sqrt{\frac{\sum(\mathrm{Y_{UAV}}-\mathrm{Y_{GPS}})^2}{\mathrm{n}}}\ ;\ \mathrm{RMSE}_z = \sqrt{\frac{\sum(\mathrm{Z_{UAV}}-\mathrm{Z_{GPS}})^2}{\mathrm{n}}} \quad (9)$$

$$\mathrm{RMSE_t} = \sqrt{(\mathrm{RMSE_x})^2 + \left(\mathrm{RMSE_y}\right)^2} \quad (10)$$

The n-th value denotes the total number of paired comparisons. It is necessary to have the plane RMSE value, which is spread in 2D X and Y directions, to compute the radial error using the standard data. The residuals' normality distribution was examined using statistical measures, including skewness and kurtosis. Error distributions were tested for normality using the Q-Q plot as well. Table 6 shows the BBA accuracy results and variances at individual GCPs for a 15-GCP configuration. 11 GCPs were used as a control reference (Table 6), whereas 4 GCPs were used as checkpoints (Table 7). However, Figure 7 shows the GCP locations and their error estimates in the ground scale delivered in three dimensions. These errors were computed based on ellipse error analysis in 3D space. They demonstrate valid and high-accuracy level validation results of the extracted photogrammetric 3D model.

Table 6: Accuracy and validation results delivered at individual GCPs (cm).

GCP. No.	Label	X error (cm)	Y error (cm)	Z error (cm)	Total error (cm)
1	GPS0001	-1.02809	1.45429	0.833638	1.96644
2	GPS0003	-0.634137	1.75483	-0.390139	1.90625
3	GPS0005	2.49043	-3.31595	0.522414	4.17979
4	GPS0006	1.49317	-2.76481	-0.767758	3.23468
5	GPS0007	0.662811	1.98615	0.051517	2.09446
6	GPS0009	0.536975	0.0780831	0.656476	0.851704
7	GPS0011	2.11858	-1.60527	0.52032	2.70851
8	GPS0012	-2.68213	0.149321	-0.833386	2.81259
9	GPS0014	-0.557246	0.768078	-1.36628	1.66349
10	GPS0015	-0.992227	0.726054	0.383068	1.28779
11	GPS0016	-1.40873	0.771195	0.367767	1.64758
Total		**1.52495**	**1.70816**	**0.691318**	**2.39191**

Table 7: RMSE of Checkpoints.

Total No. of Check Points	X error (cm)	Y error (cm)	Z error (cm)	Total error (cm)
4	2.50265	1.08262	2.2358	2.72678

The precision achieved is affected by the quantity and the distribution of GCPs. SfM automatic routine was utilized for the post-acquisition processing of all gathered photos. The obtained Total mean error was 2.72 cm; however, 2.50, 1.08, and 2.23 values were delivered in X, Y, and Z directions, respectively, which seems precise for mapping applications in similar conditions. As can be seen in Figure 8, the main cause of these variations is the manual quantity of the object locations in the photos during processing. The image resolution, quality, and the user's level of expertise affect how close to the center of each target is and how much error can cause to individual points on the ground. Furthermore, the targets must be visible in at least two photos, which was not the case in this case study.

These results have met with [31] findings which employed 10 GCPs and obtained 0.01-0.03m and 0.04m RMSE in horizontal and vertical dimensions, respectively. Further, to compare with [32] findings that evaluated the precision of RTK and PPK direct geo-referencing using a SenseFly eBee Plus UAV, the deliver RMSEs of 0.026 m, 0.035 m, and 0.082 m for X, Y, and Z, respectively. This indicates the maximum horizontal and vertical accuracies. However, [33] reported plane accuracy of 0.029-0.034m and vertical accuracy of 0.026-0.029m for RTK using an eBee RTK UAV to control direct georeferencing accuracy.

Figure 7: GCP locations and error estimates of results in the study site

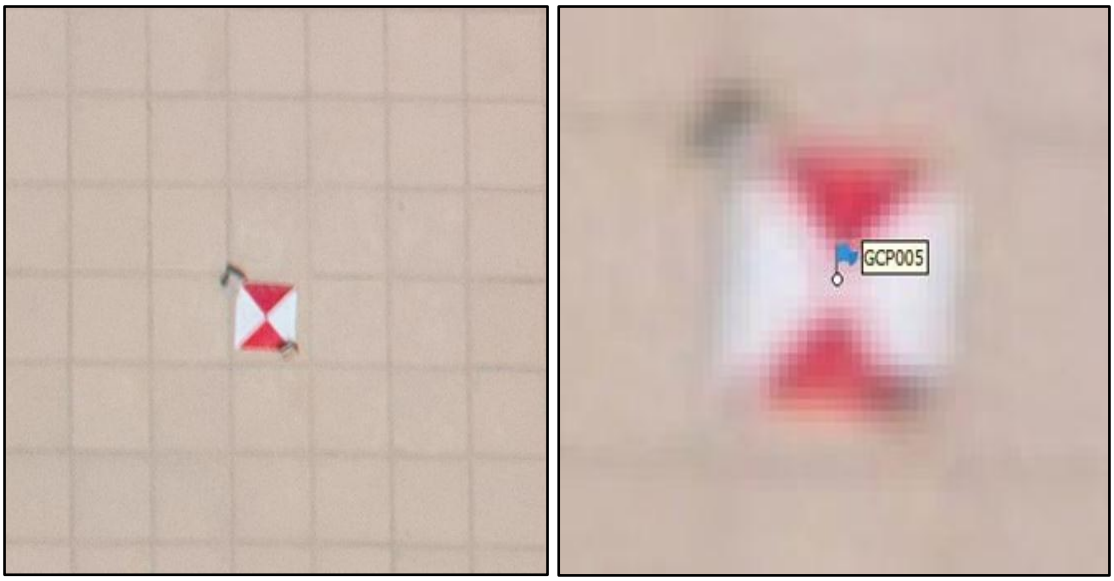

Figure 8: Target resolution in the automatic processing.

Extracting an orthomosaic map requires prior knowledge of orthophotos. The phenomenon of radial displacement, which occurs when UAVs capture photographs, distorts objects further from the image's center. Radial displacement gives the impression that a tall item's base and top were not entirely aligned or connected by a perpendicular median, which was not as pronounced with smaller objects. The method of extracting the orthophoto, orthorectification, was used to correct the radial errors obtained from individual images automatically following the photogrammetric processing pipeline in Metashape software. As can be seen from Figure 9, an orthomosaic map consists, at its most fundamental level, of a collection of orthophotos that were superimposed on one another. It seems a single image was taken from an incredibly high vantage point.

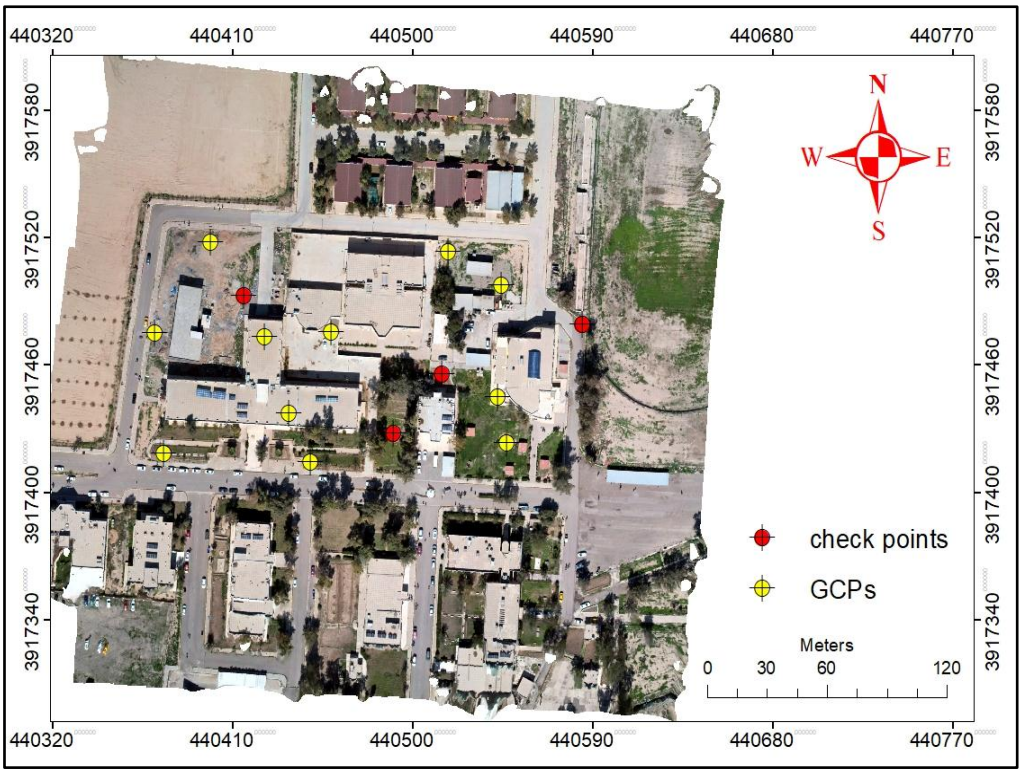

Figure 9: Orthomosaic image of the study site generated with the aid of Agisoft Metashape software.

A 3D realistic model was also extracted from the substantial point clouds dataset and used their images to create the orthophoto. Finally, the coordinates of the points in more than one image were used to create a 3D map of the region covered by overlapping photographs to deliver texture with realistic representation. Exporting processing results from the Metashape environment is possible in many forms, including dense and sparse point clouds, camera calibration and orientation data, mesh, and more. Tiled models, orthomosaics, and digital elevation models, both DSM and DTM, can all be generated to meet the user's needs, as shown in Figure 10 of this dataset.

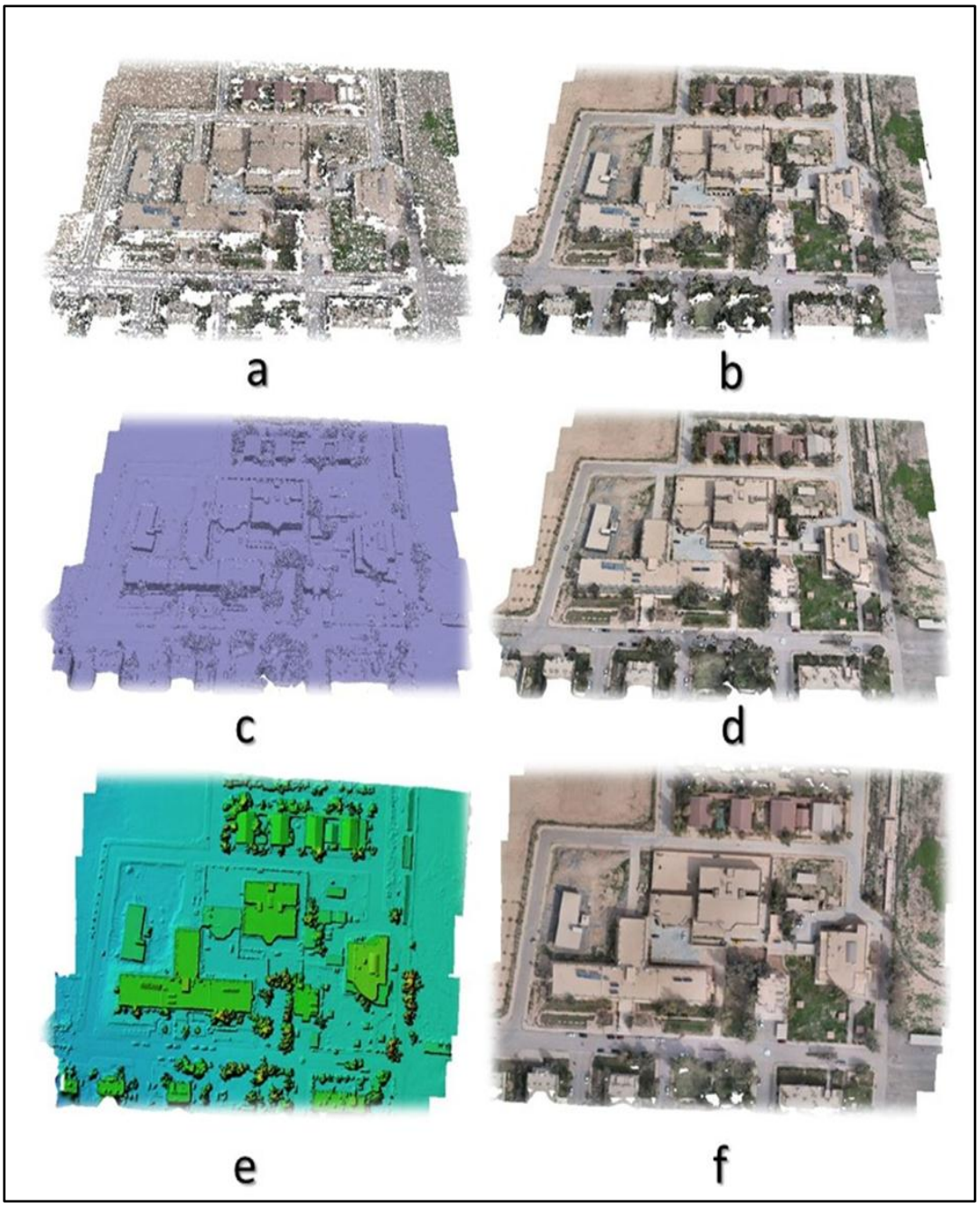

Figure 10: Output products of SfM photogrammetric workflow; (a) Spare cloud, (b) Dense cloud, (c) Mesh, (d) 3D Model, (e) DEM, (f) Orthomosic.

6. Conclusions

This study has looked into the viability of deploying a DJI Air 2s UAV to collect precise geospatial 3D data in an urban setting site for 3D mapping applications. The UAV has a 20-megapixel digital camera and a GPS that works on a single frequency, and the chosen site spans an area of around 240m×120m, making it ideal for aerial photography. The workflow was designed to optimize the flight plan parameters and ground marking configuration settings for optimal 3D mapping outputs. The ground resolution was set to 2.8cm with 60 photos captured through autopilot configuration at 100m altitude. Before collecting data, the flight plan was guaranteed at an 80% overlap percentage. Point clouds and 3D digital surface models of the surveyed region were generated with the help of the SfM-MVS

photogrammetric solution. Fifteen ground control points (GCPs) were set up at the site before the UAV imaging capture process to help determine the precision of the UAV geospatial data solution. Inside the research facility, the GCPs were dispersed and marked with large, bright Xs so the user could easily identify them at any point tagging stage within the automatic workflow. Each GCP center coordinates were measured using a Lieca viva gs15 GNSS with RTK corrections before capturing any image data. Many factors, including the geo-referencing approach, the number and distribution of ground control points, the research site's feature types, the flight plan settings, and the automatic approach utilized, can significantly impact the accuracy of the spatial data produced from UAV photogrammetry. According to mapping applications, results showed a robust accuracy following this case study's pre-plan settings and parameter optimization. Planning and building infrastructure with such detailed spatial information in future studies would be possible.

7. Conflict of Interest

The authors declare that they have no conflicts of interest.

References

[1] J. P. Dandois and E. C. Ellis, "High spatial resolution three-dimensional mapping of vegetation spectral dynamics using computer vision," *Remote Sens. Environ.*, vol. 136, pp. 259–276, 2013.

[2] S. Ahmed, A. El-Shazly, F. Abed, and W. Ahmed, "The Influence of Flight Direction and Camera Orientation on the Quality Products of UAV-Based SfM-Photogrammetry," *Appl. Sci.*, vol. 12, no. 20, 2022.

[3] P. R. Wolf, B. A. Dewitt, and B. E. Wilkinson, *Elements of Photogrammetry with Applications in GIS*. McGraw-Hill Education, 2014.

[4] X. Wang, F. Rottensteiner, and C. Heipke, "Structure from motion for ordered and unordered image sets based on random kd forests and global pose estimation," *ISPRS J. Photogramm. Remote Sens.*, vol. 147, pp. 19–41, 2019.

[5] J. Svensson and A. Andersson, "Photogrammetric 3d-mapping using low-cost unmanned aerial vehicle-Analysis of accuracy," 2018.

[6] H. H. Ali and F. M. Abed, "The impact of UAV flight planning parameters on topographic mapping quality control," in *IOP Conference Series: Materials Science and Engineering*, 2019, vol. 518, no. 2.

[7] A. X. Chang, T. Funkhouser, L. Guibas, P. Hanrahan, Q. Huang, Z. Li, S. Savarese, M. Savva, S. Song, and H. Su, "Shapenet: An information-rich 3d model repository," *arXiv preprint arXiv:1512.03012*, 2015.

[8] M. G. Ahmed and F. M. Abed, "Automatic Co-registration of UAV-Based Photogrammetry and Terrestrial Laser Scanning in Urban Areas," in *Current Trends in Geotechnical Engineering and Construction. ICGECI 2022.*, Springer, 2023, pp. 99–112.

[9] S. Kynigopoulos, "An application of augmented reality focusing on the creation of 3D models using photogrammetry." Universitat Politècnica de Catalunya, 2021.

[10] M. J. Westoby, J. Brasington, N. F. Glasser, M. J. Hambrey, and J. M. Reynolds, "'Structure-from-Motion'photogrammetry: A low-cost, effective tool for geoscience applications," *Geomorphology*, vol. 179, pp. 300–314, 2012.

[11] H. F. Difar and F. M. Abed, "Automatic Extraction of Unmanned Aerial Vehicles (UAV)-based Cadastral Map: Case Study in AL-Shatrah District-Iraq," *Iraqi J. Sci.*, vol. 63, no. 2, pp. 877–896, 2022.

[12] G. Verhoeven, "Taking computer vision aloft–archaeological three-dimensional reconstructions from aerial photographs with photoscan," *Archaeol. Prospect.*, vol. 18, no. 1, pp. 67–73, 2011.

[13] I. Kadhim and F. M. Abed, "The Potential of LiDAR and UAV-Photogrammetric Data Analysis to Interpret Archaeological Sites: A Case Study of Chun Castle in South-West England," *ISPRS Int. J. Geo-Information*, vol. 10, no. 1, p. 41, 2021.

[14] H. R. Sarhan and F. M. Abed, "The Feasibility of Using UAV Structure from Motion Photogrammetry to Extract HBIM of the Great Ziggurat of UR," *Iraqi J. Sci.*, vol. 62, no. 11, pp. 4518–4528, 2021.

[15] P. Gabrlik, A. la Cour-Harbo, P. Kalvodova, L. Zalud, and P. Janata, "Calibration and accuracy assessment in a direct georeferencing system for UAS photogrammetry," *Int. J. Remote Sens.*, vol. 39, no. 15–16, pp. 4931–4959, 2018.

[16] H. Eisenbeiss and M. Sauerbier, "Investigation of UAV systems and flight modes for photogrammetric applications," *Photogramm. Rec.*, vol. 26, no. 136, pp. 400–421, 2011.

[17] A. R. Qubaa, A. N. Hamdon, and T. A. Al Jawwadi, "Morphology Detection in Archaeological Ancient Sites by Using UAVs/Drones Data and GIS techniques," *Iraqi J. Sci.*, vol. 62, no. 11, pp. 4557–4570, 2021.

[18] F. Remondino, L. Barazzetti, F. Nex, M. Scaioni, and D. Sarazzi, "UAV photogrammetry for mapping and 3d modeling–current status and future perspectives," *Int. Arch. Photogramm. Remote Sens. Spat. Inf. Sci.*, vol. 38, no. 1, p. C22, 2011.

[19] G. Rock, J. B. Ries, and T. Udelhoven, "Sensitivity analysis of UAV-photogrammetry for creating digital elevation models (DEM)," in *Proceedings of the Conference on Unmanned Aerial Vehicle in Geomatics, Zurich, Switzerland*, 2011, vol. 1416.

[20] J. A. Gonçalves and R. Henriques, "UAV photogrammetry for topographic monitoring of coastal areas," *ISPRS J. Photogramm. Remote Sens.*, vol. 104, pp. 101–111, 2015.

[21] M. Shahbazi, G. Sohn, J. Théau, and P. Menard, "Development and evaluation of a UAV-photogrammetry system for precise 3D environmental modeling," *Sensors*, vol. 15, no. 11, pp. 27493–27524, 2015.

[22] P. Martínez-Carricondoa, F. Agüera-Vegaa, F. Carvajal-Ramíreza, F.-J. Mesas-Carrascosab, A. García-Ferrerb, and F.-J. Pérez-Porrasb, "Int J Appl Earth Obs Geoinformation," *Int J Appl Earth Obs Geoinf.*, vol. 72, pp. 1–10, 2018.

[23] E. Ferrer-González, F. Agüera-Vega, F. Carvajal-Ramírez, and P. Martínez-Carricondo, "UAV photogrammetry accuracy assessment for corridor mapping based on the number and distribution of ground control points," *Remote Sens.*, vol. 12, no. 15, p. 2447, 2020.

[24] I. Elkhrachy, "Accuracy assessment of low-cost Unmanned Aerial Vehicle (UAV) photogrammetry," *Alexandria Eng. J.*, vol. 60, no. 6, pp. 5579–5590, 2021.

[25] D. T. Booth, S. E. Cox, and G. Simonds, "Riparian monitoring using 2-cm GSD aerial photography," *Ecol. Indic.*, vol. 7, no. 3, pp. 636–648, 2007.

[26] I. Kadhim, F. M. Abed, J. M. Vilbig, and V. Sagan, "Combining Remote Sensing Approaches for Detecting Marks of Archaeological and Demolished Constructions in Cahokia s Grand Plaza, Southwestern Illinois," 2023.

[27] M. M. Costagliola-Ray *et al.*, "To fly or not to fly? Comparing vantage point and uncrewed aerial vehicle surveys for assessments of seabird abundance and fine-scale distribution," *Environ. Impact Assess. Rev.*, vol. 97, p. 106906, 2022.

[28] M. Uysal, A. S. Toprak, and N. Polat, "DEM generation with UAV Photogrammetry and accuracy analysis in Sahitler Hill," *Measurement*, vol. 73, pp. 539–543, 2015.

[29] M. R. James and S. Robson, "Straightforward reconstruction of 3D surfaces and topography with a camera: Accuracy and geoscience application," *J. Geophys. Res. Earth Surf.*, vol. 117, no. F3, 2012.

[30] H. Eisenbeiß, E. T. H. Zurich, H. Eisenbeiß, and E. T. H. Zürich, *UAV photogrammetry*, no. 18515. 2009.

[31] F. He, T. Zhou, W. Xiong, S. M. Hasheminnasab, and A. Habib, "Automated aerial triangulation for UAV-based mapping," *Remote Sens.*, vol. 10, no. 12, p. 1952, 2018.

[32] J. Tomaštík, M. Mokroš, Š. Saloň, F. Chudý, and D. Tunák, "Accuracy of photogrammetric UAV-based point clouds under conditions of partially-open forest canopy," *Forests*, vol. 8, no. 5, p. 151, 2017.

[33] M. Rabah, M. Basiouny, E. Ghanem, and A. Elhadary, "Using RTK and VRS in direct geo-referencing of the UAV imagery," *NRIAG J. Astron. Geophys.*, vol. 7, no. 2, pp. 220–226, 2018.